

# Self-Assembly of an Alkylated Guanosine Derivative into Ordered Supramolecular Nanoribbons in Solution and on Solid Surfaces

Stefano Lena,<sup>[a]</sup> Giorgia Brancolini,<sup>[c]</sup> Giovanni Gottarelli,<sup>[a]</sup> Paolo Mariani,<sup>[b]</sup> Stefano Masiero,<sup>[a]</sup> Alessandro Venturini,<sup>[c]</sup> Vincenzo Palermo,<sup>[c]</sup> Omar Pandoli,<sup>[a]</sup> Silvia Pieraccini,<sup>[a]</sup> Paolo Samorì,<sup>\*,[d]</sup> and Gian Piero Spada<sup>\*,[a]</sup>

**Abstract:** We report on the synthesis and self-assembly of a guanosine derivative bearing an alkyloxy side group under different environmental conditions. This derivative was found to spontaneously form ordered supramolecular nanoribbons in which the individual nucleobases are interacting through H-bonds. In toluene and chloroform solutions the formation of gel-like liquid-crystalline phases was observed. Sub-molecularly resolved scanning tunneling microscopic imaging of monolayers physisorbed at the

graphite–solution interface revealed highly ordered two-dimensional networks. The recorded intramolecular contrast can be ascribed to the electronic properties of the different moieties composing the molecule, as proven by quantum-chemical calculations. This self-assembly behavior is in excellent agreement with that of 5'-O-acylated

guanosines, which are also characterized by a self-assembled motif of guanosines that resembles parallel ribbons. Therefore, for guanosine derivatives (without sterically demanding groups on the guanine base) the formation of supramolecular nanoribbons in solution, in the solid state, and on flat surfaces is universal. This result is truly important in view of the electronic properties of these supramolecular anisotropic architectures and thus for potential applications in the fields of nano- and opto-electronics.

**Keywords:** guanosine • liquid crystals • nanoribbons • self-assembly • supramolecular chemistry

[a] Dr. S. Lena, Prof. G. Gottarelli, Dr. S. Masiero, O. Pandoli, Dr. S. Pieraccini, Prof. G. P. Spada  
Alma Mater Studiorum-Università di Bologna  
Dipartimento di Chimica Organica "A. Mangini"  
Via San Giacomo 11, 40126 Bologna (Italy)  
Fax: (+39)051-209-5688  
E-mail: GianPiero.Spada@unibo.it


[b] Prof. P. Mariani  
Università Politecnica delle Marche  
Dipartimento di Scienze Applicate ai Sistemi Complessi and INFN  
via Ranieri 65, 60131 Ancona (Italy)

[c] Dr. G. Brancolini, Dr. A. Venturini, Dr. V. Palermo  
Istituto per la Sintesi Organica e la Fotoreattività  
Consiglio Nazionale delle Ricerche, via Gobetti 101  
40129 Bologna (Italy)

[d] Dr. P. Samorì  
Institut de Science et d'Ingénierie Supramoléculaires  
Université Louis Pasteur  
8, allée Gaspard Monge, 67083 Strasbourg (France)  
and  
Istituto per la Sintesi Organica e la Fotoreattività  
Consiglio Nazionale delle Ricerche, via Gobetti 101  
40129 Bologna (Italy)  
Fax: (+33)390-245-161  
E-mail: samori@isis-ulp.org

## Introduction

Mimicking nature, hierarchical self-assembly<sup>[1]</sup> provides a tool for bottom-up nanoconstruction of sophisticated functional architectures<sup>[2]</sup> as for the unraveling of complex biological arrangements and processes,<sup>[3,4]</sup> paving the way towards their potential application in the realms of nanotechnology<sup>[5]</sup> and nanomedicine.<sup>[6]</sup> Self-assembly is an intrinsic property of DNA nucleosides.<sup>[3]</sup> Learning to precisely control nucleoside self-assembly represents a powerful way of constructing a wealth of complex architectures and nanostructured materials, as well as devices with pre-programmed (dynamics) functions.<sup>[7]</sup> Ultimately, one might foresee their use as components for bio-hybrid electronics,<sup>[8]</sup> such as transistors. Lipophilic guanosine nucleosides can undergo different self-assembly pathways, depending on the experimental conditions (Figure 1). The presence of monovalent and divalent cations can template the formation of G-quadruplex-based octamers or columnar aggregates, depending on the concentration of the ion and nucleobase, both for organic-soluble<sup>[9,10]</sup> and water-soluble derivatives.<sup>[11]</sup> These G quadruplexes are of great interest because they hold potential in anticancer drug design as they can act as enzyme telo-

 Supporting information for this article is available on the WWW under <http://www.chemeurj.org/> or from the author.

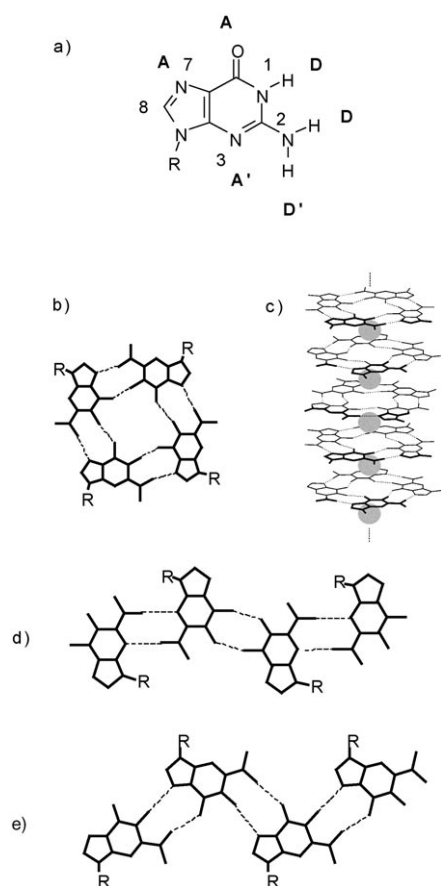


Figure 1. a) Donor/acceptor sites in the guanine moiety, b) the G-quartet arrangement, c) the ion-directed columnar self-assembly, d) and e) the structural motifs of the two ribbon-like supramolecular assemblies of guanosine derivatives in the absence of cations.

merase inhibitors.<sup>[12]</sup> Surprisingly the formation of G quadruplexes was also accomplished in the absence of cations by grafting a sterically demanding group to the C(8) position, which induced a *syn* stereochemistry.<sup>[13]</sup>

In the absence of metal templates, guanosines without a C(8) substituent self-assemble, both in solution and in the solid state, into ribbon-like architectures with an *anti* orientation of the base around the glycosidic bond.<sup>[10,14–16]</sup> These ribbon structures are interesting as they are the building blocks for new lyotropic mesophases formed in organic solvents.<sup>[15,17]</sup> In the solid state the ribbons, by bridging gold electrodes, are photoconductive.<sup>[18]</sup> More interestingly, these ribbons also display rectifying properties.<sup>[19]</sup> A field-effect transistor based on this supramolecular structure has recently been described.<sup>[20]</sup> It is worth noting that the ribbon shown in Figure 1e is dipolar and that in the crystal, owing to the parallel packing of the ribbons, these dipoles are parallel.<sup>[15]</sup>

Araki and Yoshikawa recently introduced nonpolar and flexible alkylsilyl groups into 2'-deoxyguanosine to obtain efficient organogelators for alkanes.<sup>[21]</sup> From an in-depth structural analysis, they concluded that in these gels the basic structure is a sheetlike assembly: the supramolecular

structure (see Figure 2) consists of anti-parallel G ribbons like in Figure 1e linked through two additional inter-tape hydrogen bonds between NH(2) and N(3) of the two guanines belonging to adjacent ribbons. Upon heating, a gel-to-liquid-crystal phase transition is observed and has been ascribed to the selective cleavage of the inter-tape H-bonds.

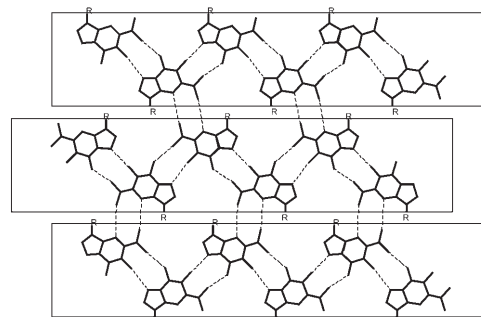
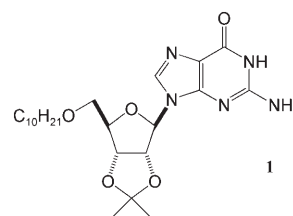


Figure 2. Two-dimensional H-bonded sheet of guanine moieties. The boxes highlight the individual guanine ribbons (see Figure 1e) connected by H-bonds between NH(2) and N(3) of two facing guanines belonging to adjacent ribbons.<sup>[16]</sup>

In our attempts to find general strategies to form guanosine nanoribbons, we never observed this sheet-like architecture for 5'-*O* acylated guanosines. To verify the universality of the tendency for guanosine derivatives to form ribbonlike motifs irrespective of the nature of the 5'-*O* substitution, we prepared the *O*-alkylated guanosine **1**. Our specific goal was to find out if the carbonyl group in the 5'-*O*-acylated derivative, which is known to interact through an intra-ribbon H-bond with NH(2), was essential for the formation of nanoribbons. It is worth stressing that the strongly anisotropic quasi-1D nanoribbons were found to possess interesting physicochemical properties,<sup>[18–20]</sup> while the 2D sheetlike assemblies can be expected to hold different yet more modest properties for applications in (opto)electronics. In light of this, it is of paramount importance to find universal strategies to form functional nanoribbons from different guanosine derivatives in order to control and improve the properties of the supramolecular arrangements. We report here on the synthesis, solution characterization, and self-assembly of **1**; small-angle X-ray diffraction characterization made it



possible to study the structure in the liquid-crystalline phases, scanning tunneling microscopy investigations, corroborated by quantum chemical calculation, were employed to unveil the structural and electronic properties of the self-assembled species on graphite.

## Results and Discussion

**Self-assembly in solution:** The supramolecular behavior of compound **1** was studied by NMR spectroscopy. Spectra were recorded at room temperature in  $\text{CDCl}_3$  and  $[\text{D}_6]\text{DMSO}/\text{CDCl}_3$  3:1 solutions with concentrations ranging from  $8 \times 10^{-3}$  to  $7 \times 10^{-2}$  M. Signals (Table 1) were assigned on the basis of 2D COSY and NOESY experiments.

Table 1.  $^1\text{H}$  NMR (400 MHz) chemical shifts (ppm) for solutions of **1** at RT. Assignments were made on the basis of COSY and NOESY spectra.

<i>c</i> (solvent)	NH(1)	H(8)	NH(2)	H(1')	H(2')	H(3')	H(4')	H(5'/5'') <sup>[a]</sup>	OCH <sub>2</sub>	isopropylidene CH <sub>3</sub> <sup>[a]</sup>
$8 \times 10^{-3}$ M ( $\text{CDCl}_3$ )	12.02	7.76	6.01	6.02	5.15	4.92	4.43	3.64–3.57	3.43	1.62–1.39
$3 \times 10^{-2}$ M ( $\text{CDCl}_3$ )	12.02	7.76	6.25	6.02	5.18	4.92	4.42	3.62–3.57	3.43	1.62–1.39
$7 \times 10^{-2}$ M ( $\text{CDCl}_3$ )	12.02	7.77	6.28	6.02	5.18	4.92	4.42	3.63–3.57	3.43	1.62–1.39
$5 \times 10^{-2}$ M ( $[\text{D}_6]\text{DMSO}/\text{CDCl}_3$ )	10.64	7.73	6.17	5.91	5.03	4.90	4.27	3.55–3.48	3.35	1.49–1.28

[a] Diastereotopic protons have not been assigned.

Modest line broadening was observed upon increasing the concentration in  $\text{CDCl}_3$ . The proton spectrum in  $[\text{D}_6]\text{DMSO}/\text{CDCl}_3$  shows the NH(1) signal at  $\delta = 10.64$  ppm. This signal shifts to  $\delta = 12.02$  ppm in pure  $\text{CDCl}_3$  solutions and is unaffected when the concentration is increased from  $8 \times 10^{-3}$  to  $7 \times 10^{-2}$  M. The NH(2) signal appears as a broad singlet at  $\delta = 6.17$  and 6.01 ppm in  $[\text{D}_6]\text{DMSO}/\text{CDCl}_3$  and in the most diluted  $\text{CDCl}_3$  solution, respectively, and shifts slightly downfield with increasing concentration in chloroform ( $\delta = 6.28$  ppm for the  $7 \times 10^{-2}$  M solution). The NH(1) group therefore always seems to be hydrogen-bonded in chloroform, while the NH(2) is eventually hydrogen-bonded only at higher concentration. While NOESY spectra recorded for the most dilute solutions in  $\text{CDCl}_3$  and in DMSO show cross peaks with phases opposite to the diagonal, solutions above  $3 \times 10^{-2}$  M exhibit cross peaks with the same phase as the diagonal. Therefore, in the lower concentration range in chloroform the aggregates are still in the fast-tumbling regime<sup>[22]</sup> and no extensive hydrogen bonding seems to occur. Given that the molecular weight of **1** is 463, and considering the downfield shift observed for the NH(1) proton in  $\text{CDCl}_3$  relative to the signal in DMSO, we can conclude that the compound exists as a dimer in dilute chloroform solution, as observed before<sup>[14]</sup> for a similar compound. At higher concentrations the scenario is markedly different: with increasing concentration we observed the formation of supramolecular oligomeric/polymeric aggregates with higher “molecular” weight and slower tumbling rates, as evidenced by negative cross peaks in the NOESY spectra.

Information on the structure of supramolecular aggregates can be gathered from a closer inspection of NOESY and ROESY spectra. In Figure 3 the NOESY spectrum of a

$7 \times 10^{-2}$  M solution of **1** in  $\text{CDCl}_3$  (mixing time 100 ms) is reported. The spectrum shows cross peaks (boxed) between NH(1) and H(8) and between NH(2) and H(8) signals. These signals are characteristic of the ribbon-like supramolecular arrangement shown in Figure 1e.<sup>[14]</sup> It is noteworthy that cross peaks between NH(2) and H(2') or H(1') signals are very weak and cross peaks between isopropylidene  $\text{CH}_3$  and NH(2) signals are absent. These last interactions would be expected both if the supramolecular structure were of the type depicted in Figure 1d or in the case of a sheetlike assembly analogous to the one described by Araki and co-workers (Figure 2). It should be pointed out that proton spectra did not change with time and that NOESY spectra were recorded on aged samples in wet  $\text{CDCl}_3$ : under these same conditions, the analogous didecanoyl ester derivative<sup>[14]</sup> self-assembles through the hydrogen-bond network shown in Figure 1d.

The CD spectrum of **1** in chloroform shows (see Supporting Information) weak signals in the 300–220 nm wavelength region corresponding to the low-energy transitions of the guanine chromophore. This behavior is in agreement with previous reports on ribbon-forming guanosines<sup>[15]</sup> in contrast with helix-forming guanosines, which give relatively intense CD, as reported for 8-oxoguanosine derivatives.<sup>[23,24]</sup>

**The liquid-crystalline phase:** Compound **1** exhibits lyotropic liquid-crystalline properties in organic solvents. Polarized optical microscopy (POM) reveals the presence of a birefringent fluid phase at  $c > 2.5\%$  (*w/w*) in toluene and chloroform (Figure 4).

X-Ray diffraction experiments confirm the existence of a liquid-crystalline order. Compound **1** was investigated in toluene and in chloroform at different concentrations and in the form of a dry film produced by drop-casting chloroform solutions. While diffraction spectra in chloroform solutions were very low in intensity (due to chloroform absorption), one or two intense peaks in the low-angle region and a large band in the high-angle region were detected in toluene solutions.

Better-resolved X-ray diffraction profiles were obtained at concentrations higher than 50% (*w/w*) or by using the dry film cast from chloroform solution. A typical X-ray diffraction pattern is supplied in the Supporting Information. In particular, the low-angle diffraction region is characterized by a series of broad peaks that can be indexed according to a 2D rectangular lattice of  $p2mm$  symmetry.<sup>[25]</sup> From the Bragg spacings  $Q_{h,k}$ , the unit cell dimensions *a* and *b* have been derived using Equation (1), in which *h* and *k* are the Miller indices of the observed Bragg reflections. The

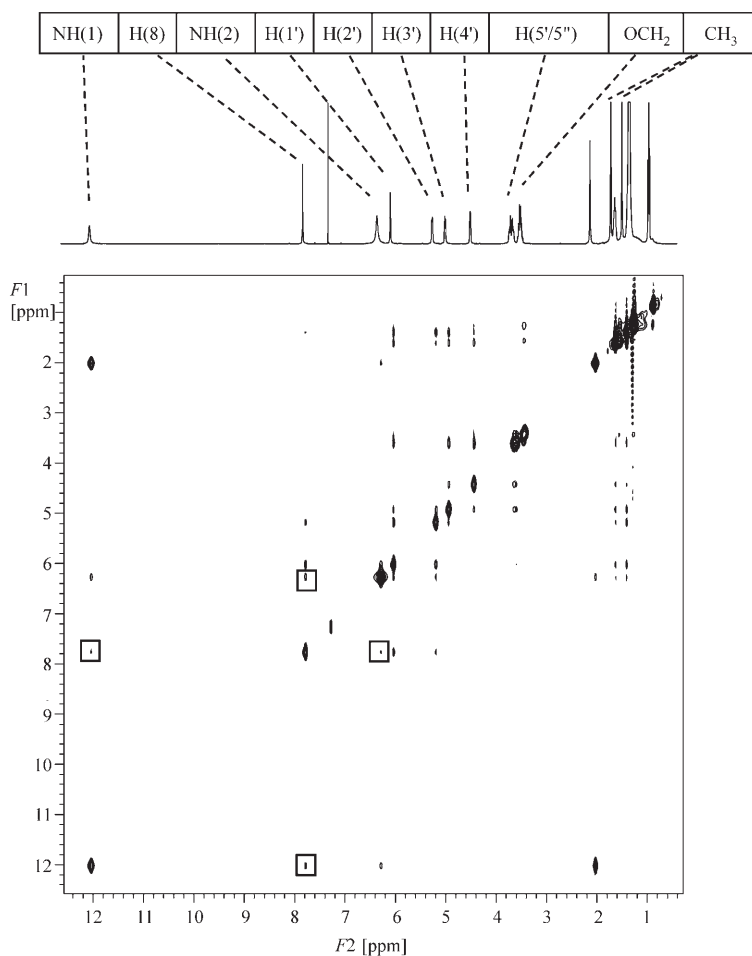


Figure 3. NOESY spectrum (mixing time 100 ms) of  $7 \times 10^{-2}$  M **1** in  $\text{CDCl}_3$  at RT. Relevant intermolecular cross-peaks are boxed.

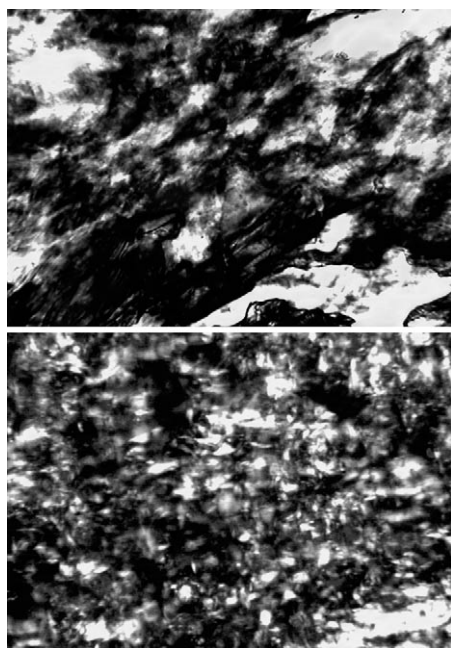


Figure 4. Polarized optical microscopy images of 7% (w/w) solutions of **1** in toluene (top) and chloroform (bottom). Magnification  $100\times$ .

unit cell parameters show a dependence on concentration (see Table 2), while a rather small unit cell has been derived for the dry film.

$$Q_{h,k} = 2\pi((h/a)^2 + (k/b)^2)^{0.5} \quad (1)$$

The high-angle diffraction region is characterized by two bands, the first rather narrow and centered at about  $Q = (5.46 \text{ \AA})^{-1}$ , while the second is very large and centered at  $Q = (4.5 \text{ \AA})^{-1}$ . Both peak positions are insensitive to the toluene concentration.

The X-ray diffraction profiles are thus consistent with the presence of a liquid-crystalline phase:<sup>[26]</sup> the low-angle peaks suggest a 2D rectangular packing of aggregates, whose distance depends on the amount of solvent. According to the symmetry group, two aggregates are present in the unit cell (see Figure 5). On the other hand, the high-angle large band indicates the disordered conformation of the hydrocarbon chains (eventually dissolved in the solvent), while

the narrow band provides evidence for an intra-aggregate characteristic repeat distance of 5.5 Å.

From the unit cell parameters, the cross-sectional area  $S_{\text{core}}$  of the central core of the aggregates can be determined, assuming that they are infinite in length and that the unit cell can be divided into two regions, one holding the guano-

Table 2. Low-angle X-ray diffraction results.  $A$  and  $b$  are the parameters of the 2D rectangular unit cell,  $c$  is the weight of **1** over the total weight of the sample,  $S_{\text{core}}$  is the cross-sectional area of the central core of the ribbon (see text).

$a$ [Å, $\pm 0.5$ ]	$b$ [Å, $\pm 0.5$ ]	$c$ [w/w, $\pm 5\%$ ]	$S_{\text{core}}$ [Å <sup>2</sup> , $\pm 10\%$ ]
25.9	9.8	1.0	78.0
28.7	10.0	0.9	79.4
32.0	11.5	0.75	84.9
36.7	11.7	0.6	79.9
38.0	12.0	0.5	70.1
40.2	— <sup>[a]</sup>	0.4	—
43.5	— <sup>[a]</sup>	0.3	—
44.6	— <sup>[a]</sup>	0.2	—
46.1	— <sup>[a]</sup>	0.1	—

[a] Only one peak is detected at low concentration, therefore the  $b$  parameter cannot be determined.

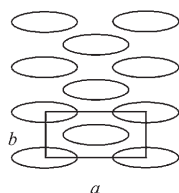


Figure 5. Geometrical model for the 2D-rectangular phase. The cross section of the aggregates is represented as an ellipsoid.

sine residues and the other the alkyl chains together with the organic solvent.<sup>[15]</sup> The relation between  $S_{\text{core}}$  and the 2D rectangular unit cell surface is given in Equation (2),<sup>[26]</sup> in which  $c_{\text{v,G}}$  is the volume concentration of the guanosine residue inside the unit cell volume.

$$2S_{\text{core}} = a \cdot b \cdot c_{\text{v,G}} \quad (2)$$

In the special case when the solvent is absent,  $c_{\text{v,G}}$  corresponds to the volume fraction of the guanosine residue ( $V_{\text{G}}=470 \text{ \AA}^3$ ) with respect to the molecular volume ( $V=770 \text{ \AA}^3$ ) calculated from standard atomic dimensions. A cross-section of about  $80 \text{ \AA}^2$  has been calculated (see Table 2), independent of the toluene concentration. The cross-sectional area of the guanosine core of the ribbon calculated from molecular models is indeed around  $70 \text{ \AA}^2$ , very similar to the experimentally derived values.

According to our previous results,<sup>[15]</sup> the observed data and the behavior detected as a function of concentration are consistent with the occurrence of a phase in which the structure elements are ribbons, infinite in length and parallel to each other, packed in a 2D-rectangular lattice. The ribbons contain the guanine residues in the extended hydrogen-bonded configuration, while the alkyl chains, together with the organic solvent in which they are dissolved, fill the lateral gap between the ribbons. The diffuse band observed at  $Q=(4.5 \text{ \AA})^{-1}$  is characteristic of liquid paraffins, and indicates a disordered (liquid-like) organization within the hydrocarbon region.<sup>[15,23]</sup> As the solvent is expected to scatter in the same  $Q$  region, no detailed information on the hydrocarbon conformation can be derived. On the basis of the ribbon structures reported in Figure 1, the peak centered at  $Q = (5.5 \text{ \AA})^{-1}$  could be related to the guanosine repeat distance within the ribbon.

**Self-assembly at the solid-liquid interface:** Given the interesting results obtained on the self-assembly of **1** in solution as observed with indirect methods, we extended our studies to STM to provide mapping in real space. In fact, STM imaging offers sub-molecularly resolved imaging of the local density of states (LDOS) of a molecular adsorbate at the surface.<sup>[27]</sup> The high resolution that can be achieved by STM enables discrimination between different chemical functionalities adsorbed at surfaces.<sup>[28]</sup> STM was successfully employed in an ultra-high vacuum environment to investigate guanine-based architectures in which single units are interacting through H-bonds to form quadruplexes on Au(111),

which were found to be stabilized by resonance-assisted hydrogen bonding.<sup>[29]</sup> The unique versatility of STM enables the in situ exploration of the self-assembly of an organic molecule at the interface between its own solution in a poorly polar solvent and a solid conductive substrate.<sup>[30]</sup>

Figure 6 displays a high-resolution STM image of **1** self-assembled at the graphite-solution interface. This STM current image reveals a 2D crystalline lamellar structure with a rectangular periodic motif. The determined cell parameters are  $a=2.20 \pm 0.20$ ,  $b=1.43 \pm 0.15 \text{ nm}$ ,  $\alpha=83 \pm 4^\circ$ .

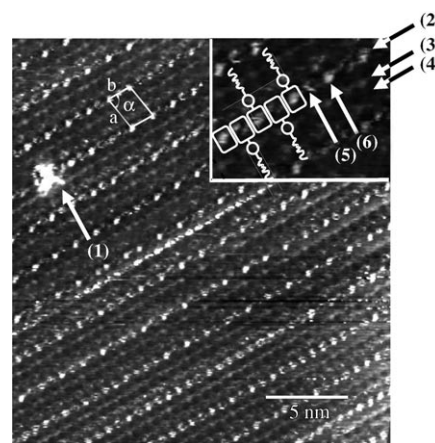


Figure 6. STM current image of **1** at the graphite-solution interface using trichlorobenzene as the solvent. Bias voltage ( $U_t$ ) = 400 mV and average tunneling current ( $I_t$ ) = 30 pA. Arrow 1 marks a defect probably due to a disordered cluster adsorbed on the self-assembled monolayer. Inset (top, right) shows the zoom-in highlighting the three different types of contrast in a row: guanine core (arrow 2), ribose (arrow 3) and aliphatic tails (arrow 4). Two adjacent guanines, linked by H-bonds, appear with different contrasts as marked by arrows 5 and 6. A cartoon of the H-bonded network is shown in the inset: the rectangles represent the guanine bases, the circles stand for the sugars, and the aliphatic tails are sketched with lines.

Assuming resonant tunneling between the frontier orbitals of the moieties at surfaces and the Fermi level of the substrate as the dominant mechanism for contrast formation in STM measurements, the probability for electrons to tunnel from occupied states of the substrate to the unoccupied states of the adsorbates depends on the energy gap between them. In view of this we have performed quantum-chemical calculations to estimate the energy of the frontier orbitals of the moieties composing our molecular system, that is, the highest occupied (HOMO) and the lowest unoccupied molecular orbitals (LUMO), and we have compared them with the Fermi level of the graphite substrate. The results are summarized in Figure 7. Because the experimental results were obtained in the condensed phase, for the interpretation of the STM contrasts they have to be considered only for the trend in the energy differences of the levels.

In our current STM image, the brightest spots, which are marked with arrow 2 in the inset in Figure 6, can be attributed to the guanine cores, since the energy difference between their HOMO and the Fermi level of the graphite substrate

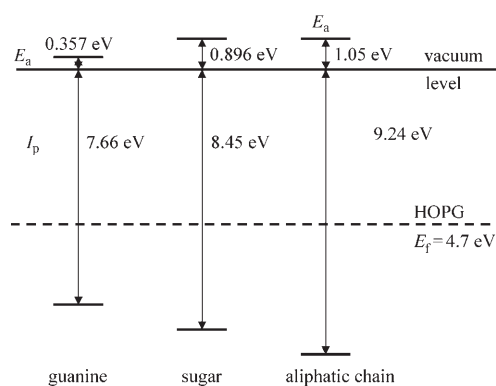


Figure 7. Scheme of the adiabatic electron affinities ( $E_a$ ) and ionization potentials ( $I_p$ ) for guanine, sugar, and aliphatic chain ( $C_{10}H_{22}$ ) in vacuo, as calculated from energy differences between the optimized structures of neutral and charged systems at the B3LYP/6-311+G\*\*//B3LYP/6-31G\* level of theory.

is rather small.<sup>[31]</sup> Spots with a lower brightness, indicated with arrow 3, can be ascribed to the ribose, while the darker part of the image (arrow 4) can be attributed to the aliphatic side chains, which have not been resolved, probably owing to their high conformational mobility on a time scale faster than the STM imaging. Therefore the detailed analysis assisted by quantum-chemical calculations made it possible to discriminate different moieties composing **1**.

A careful inspection reveals that the contrast of two adjacent guanines linked by H-bonding is different (see, for example, those marked by arrows 5 and 6 in Figure 6); this can be explained in view of a different packing in the  $X,Y$  with respect to the HOPG lattice underneath. The value of the cell parameter  $a$ , which roughly amounts to half of the estimated ribbon width, suggests that the alkyl tails in two adjacent H-bonded ribbons are interdigitated. Given the STM resolution obtained, and in view of the pretty similar size of the unit cell that can be expected for the two nanoribbons depicted in Figures 1d and e, taking into account the estimated unit cell and relative error bar, we are unable to unambiguously ascribe the supramolecular motif shown in Figure 6 to either one or the other nanoribbon-type.

On a larger scale, a monolayer of **1** is polycrystalline (see Figure 8). Up to seven domains with a diameter of a few tens of nanometers are observed. The orientation of most of the lamellae is symmetry-equivalent with respect to the crystalline substrate lattice. The high-resolution imaging achieved in the polycrystalline structure made it possible to record two different kinds of defects on the nanometer length scale. The first kind of defect consists of empty domains in which the molecules are not adsorbed at surfaces; an example of missing molecules is indicated by a grey arrow. Such defects get recovered on the time scale of a few minutes. The second kind of defect is found at the domain boundaries, which have a fuzzy character and surround some crystals (marked with white arrows). At these frontiers the molecules are more loosely packed.

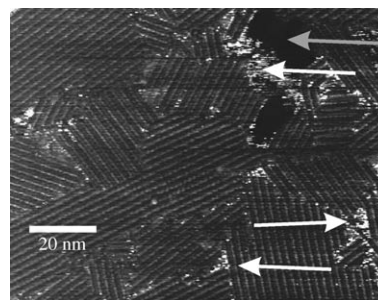


Figure 8. Current STM survey image of self-assembled architecture of **1** recorded at the solid-liquid interface on HOPG.  $U_t = 290$  mV and average  $I_t = 200$  pA.

## Conclusion

In summary, in our attempt to find general strategies to form functional nanoribbons from guanosine derivatives, we have prepared *O*-alkylated guanosine, which is an extension of the well-known 5'-*O*-acylated guanosines. Our specific goal was to find out if the carbonyl group, existing in the 5'-*O*-acylated derivative, which is known to interact through an intra-ribbon H-bond with NH(2), was essential for the formation of nanoribbons. We have thus synthesized and studied the self-assembly of **1** under different environmental conditions. NMR, X-ray, and STM measurements revealed that **1** self-assembles into highly ordered nanoribbons in which the single nucleosides are held together by H-bonds. This self-assembly behavior appears to be universal, as it is in line with many other guanosine derivatives, and in particular with that of 5'-*O*-acylated guanosines, revealing that the presence of the carbonyl unit in the 5'-*O*-acylated derivative is not a prerequisite for the formation of the nanoribbon. The self-assembled motif observed for **1** conveys parallel ribbons, most probably with parallel dipoles. This result is very important in view of the well-known physico-chemical properties of these quasi-1D nanostructures, and in particular for their use in (opto)electronics.

## Experimental Section

**2',3'-*O*-Isopropylidene-5'-*O*-decylguanosine:** 2',3'-*O*-Isopropylidene-guanosine (Sigma) (0.4 g, 1.2 mmol) was dried in vacuo over  $P_2O_5$  for 2 h at 50 °C and suspended in anhydrous THF (10 mL). NaH (0.058 g, 2.4 mmol) and 1-bromodecane (1.24 mL, 6 mmol) were added. The mixture was heated at reflux overnight, then cooled to room temperature. The solvent was removed and the residual solid was taken up in dichloromethane, washed with water, dried over  $MgSO_4$ , concentrated in vacuo, and applied to a silica gel column using 94:6 dichloromethane/methanol as the eluent. The product was recrystallized from ethanol to afford a white solid (0.26 g, 48% yield).  $^1H$  NMR (400 MHz,  $CDCl_3$ ):  $\delta = 0.86$  (t, 3H;  $CH_3$ ), 1.25 (m, 14H;  $CH_2$ ), 1.39 (s, 3H;  $CH_3$ ), 1.53 (m, 2H;  $O-CH_2CH_2$ ), 1.61 (s, 3H;  $CH_3$ ), 3.43 (m, 2H;  $O-CH_2$ ), 3.55–3.64 (m, 2H;  $H5'-H5''$ ), 4.42 (m, 1H;  $H4'$ ), 4.92 (m, 1H;  $H3'$ ), 5.17 (m, 1H;  $H2'$ ), 6.00 (d, 1H;  $H1'$ ), 6.28 (s, 2H;  $NH_2$ ), 7.76 (s, 1H;  $H8$ ), 12.02 ppm (s, 1H;  $NH$ );  $^{13}C$  NMR (300 MHz,  $[D_6]DMSO$ ):  $\delta = 13.93$  ( $CH_3$ ), 22.07 ( $CH_2$ ), 25.21 ( $CH_3$ ), 25.53 ( $CH_2$ ), 26.98 ( $CH_3$ ), 28.68 ( $CH_2$ ), 28.30 ( $CH_2$ ), 28.93 ( $CH_2$ ), 28.97 ( $CH_2$ ), 28.99 ( $CH_2$ ), 31.28 ( $CH_2$ ), 70.43 ( $CH_2$ ), 70.61 ( $CH_2$ ),

81.44 (CH), 83.68 (CH), 84.99 (CH), 88.56 (CH), 113.01 (C), 116.76 (C), 135.69 (CH), 150.67 (C), 153.64 (C), 156.68 ppm (C); elemental analysis calcd (%) for C<sub>23</sub>H<sub>37</sub>N<sub>5</sub>O<sub>5</sub>: C 59.59, H 8.04, N 15.11; found: C 59.16, H 7.71, N 15.48.

CD spectra were recorded with a JASCO J-710 spectropolarimeter using cells of the appropriate path length. NMR spectra were recorded with Varian Mercury instruments at 300 or 400 MHz.

X-ray diffraction experiments were performed using a Philips PW1830 X-ray generator equipped with a Guinier-type focusing camera operating in a vacuum: a bent quartz crystal monochromator was used to select the Cu<sub>Kα1</sub> radiation ( $\lambda = 1.54 \text{ \AA}$ ). The investigated  $Q$  range ( $Q = (4\pi\sin\theta)/\lambda$ , where  $2\theta$  is the full scattering angle) was between 0.068 and  $2.3 \text{ \AA}^{-1}$ . Diffraction patterns were recorded on a stack of two Kodak DEF-392 films: film densities were measured using a digital scanner.

STM experiments were carried out at ambient pressure and room temperature at the solid-liquid interface. Almost saturated solutions in 1,2,4-trichlorobenzene (Aldrich) were applied to the basal plane of the highly oriented pyrolytic graphite (HOPG) substrate (Advanced Ceramics, ZYH grade). Mechanically cut Pt/Ir (80%/20%) tips were employed. The STM images of the molecules were recorded in current mode with scan rates of about  $20\text{--}50 \text{ lines s}^{-1}$ . The measurements were carried out using a picoAmp-Nanoscope IIIa Multimode set-up (Digital Instruments, Santa Barbara, CA) using a positive tip bias. The high-resolution image was corrected for thermal drift with respect to the HOPG lattice.

Adiabatic electronic affinities and ionization potentials for the molecules were evaluated as differences between the total energies of the optimized neutral and the corresponding optimized ions. The total energies and equilibrium geometries for the neutral and ionic species were obtained from full density functional optimizations at the 6-31g\* level (B3LYP/6-31g\*) using the Gaussian 03 program. Single-point energies at B3LYP/6-31g\*/B3LYP/6-31g\* were carried out to determine more accurate energy values.<sup>[32]</sup>

## Acknowledgements

This work has been supported by MUR/PRIN project "Modellazione e caratterizzazione di cristalli liquidi per strutture nano-organizzate" (2005035119), MUR/FIRB project "NOMADE" (RNNE01YSR8\_004), the University of Bologna, the ESF-SONS (BIONICS project), the Marie Curie EST project SUPER (MEST-CT-2004-008128), and the Regione Emilia-Romagna (PRIITT Nanofaber Net-Lab).

- [1] Special issue, in *Science*, Vol. 295, **2002**, pp. 2395.
- [2] F. J. M. Hoeben, P. Jonkheijm, E. W. Meijer, A. Schenning, *Chem. Rev.* **2005**, *105*, 1491; A. C. Grimsdale, K. Müllen, *Angew. Chem.* **2005**, *117*, 5732; *Angew. Chem. Int. Ed.* **2005**, *44*, 5592; J. A. A. W. Elemans, A. E. Rowan, R. J. M. Nolte, *J. Mater. Chem.* **2003**, *13*, 2661; R. Maoz, S. R. Cohen, J. Sagiv, *Adv. Mater.* **1999**, *11*, 55; M. A. B. Block, C. Kaiser, A. Khan, S. Hecht, *Top. Curr. Chem.* **2005**, *245*, 89; S. I. Stupp, V. LeBonheur, K. Walker, L. S. Li, K. E. Huggins, M. Keser, A. Amstutz, *Science* **1997**, *276*, 384; S. Onclin, B. J. Ravoo, D. N. Reinhoudt, *Angew. Chem.* **2005**, *117*, 6438; *Angew. Chem. Int. Ed.* **2005**, *44*, 6282.
- [3] E. Winfree, F. R. Liu, L. A. Wenzler, N. C. Seeman, *Nature* **1998**, *394*, 539.
- [4] E. A. Meyer, R. K. Castellano, F. Diederich, *Angew. Chem.* **2003**, *115*, 4254; *Angew. Chem. Int. Ed.* **2003**, *42*, 1210; A. Bianco, K. Kostarelos, C. D. Partidos, M. Prato, *Chem. Commun.* **2005**, 571; K. Kinbara, T. Aida, *Chem. Rev.* **2005**, *105*, 1377.
- [5] C. Joachim, J. K. Gimzewski, A. Aviram, *Nature* **2000**, *408*, 541; I. W. Hamley, *Angew. Chem.* **2003**, *115*, 1730; *Angew. Chem. Int. Ed.* **2003**, *42*, 1692; F. Rosei, *J. Phys. Condens. Matter* **2004**, *16*, S1373; M. Ferrari, *Nat. Rev. Cancer* **2005**, *5*, 161; D. M. Vriezema, M. C. Aragonés, J. A. A. W. Elemans, J. Cornelissen, A. E. Rowan, R. J. M. Nolte, *Chem. Rev.* **2005**, *105*, 1445; A. H. Flood, J. F. Stoddart, D. W. Steuerman, J. R. Heath, *Science* **2004**, *306*, 2055.
- [6] G. A. Silva, C. Czeisler, K. L. Niece, E. Beniash, D. A. Harrington, J. A. Kessler, S. I. Stupp, *Science* **2004**, *303*, 1352; S. M. Moghimi, A. C. Hunter, J. C. Murray, *FASEB J.* **2005**, *19*, 311.
- [7] P. W. K. Rothemund, *Nature* **2006**, *440*, 297.
- [8] D. Porath, G. Cuniberti, R. Di Felice, *Top. Curr. Chem.* **2004**, *237*, 183.
- [9] A. L. Marlow, E. Mezzina, G. P. Spada, S. Masiero, J. T. Davis, G. Gottarelli, *J. Org. Chem.* **1999**, *64*, 5116; S. L. Forman, J. C. Fettingter, S. Pieraccini, G. Gottarelli, J. T. Davis, *J. Am. Chem. Soc.* **2000**, *122*, 4060; X. Shi, J. C. Fettingter, J. T. Davis, *Angew. Chem.* **2001**, *113*, 2909; *Angew. Chem. Int. Ed.* **2001**, *40*, 2827; A. Wong, J. C. Fettingter, S. L. Forman, J. T. Davis, G. Wu, *J. Am. Chem. Soc.* **2002**, *124*, 742; X. Liu, I. C. M. Kwan, S. Wang, G. Wu, *Org. Lett.* **2006**, *8*, 3685; V. Gubala, D. De Jesús, J. M. Rivera, *Tetrahedron Lett.* **2006**, *47*, 1413; E. Mezzina, P. Mariani, R. Itri, S. Masiero, S. Pieraccini, G. P. Spada, F. Spinuzzi, J. T. Davis, G. Gottarelli, *Chem. Eur. J.* **2001**, *7*, 388.
- [10] J. T. Davis, G. P. Spada, *Chem. Soc. Rev.* **2007**, *36*, DOI: 10.1039/b600282j.
- [11] C. Kang, X. H. Zhang, R. Ratliff, R. Moyzis, A. Rich, *Nature* **1992**, *356*, 126; G. Laughlan, A. I. H. Murchie, D. G. Norman, M. H. Moore, P. C. E. Moody, D. M. J. Lilley, B. Luisi, *Science* **1994**, *265*, 520; F. W. Smith, J. Feigon, *Nature* **1992**, *356*, 164; F. W. Smith, F. W. Lau, J. Feigon, *Proc. Natl. Acad. Sci. USA* **1994**, *91*, 10546.
- [12] J. T. Davis, *Angew. Chem.* **2004**, *116*, 684; *Angew. Chem. Int. Ed.* **2004**, *43*, 668; T. de Lange, *Science* **1998**, *279*, 334; W. C. Hahn, C. M. Counter, A. S. Lundberg, R. L. Beijersbergen, M. W. Brooks, R. A. Weinberg, *Nature* **1999**, *400*, 464; E. S. Baker, J. T. Lee, J. L. Sessler, M. T. Bowers, *J. Am. Chem. Soc.* **2006**, *128*, 2641.
- [13] J. L. Sessler, M. Sathiosatham, K. Doerr, V. Lynch, K. A. Abboud, *Angew. Chem.* **2000**, *112*, 1356; *Angew. Chem. Int. Ed.* **2000**, *39*, 1300.
- [14] G. Gottarelli, S. Masiero, E. Mezzina, S. Pieraccini, J. P. Rabe, P. Samori, G. P. Spada, *Chem. Eur. J.* **2000**, *6*, 3242.
- [15] T. Giorgi, F. Grepioni, I. Manet, P. Mariani, S. Masiero, E. Mezzina, S. Pieraccini, L. Saturni, G. P. Spada, G. Gottarelli, *Chem. Eur. J.* **2002**, *8*, 2143.
- [16] K. Araki, R. Takasawa, I. Yoshikawa, *Chem. Commun.* **2001**, 1826.
- [17] G. Gottarelli, S. Masiero, E. Mezzina, S. Pieraccini, G. P. Spada, P. Mariani, *Liq. Cryst.* **1999**, *26*, 965; T. Kato, *Science* **2002**, *295*, 2414.
- [18] R. Rinaldi, E. Branca, R. Cingolani, S. Masiero, G. P. Spada, G. Gottarelli, *Appl. Phys. Lett.* **2001**, *78*, 3541.
- [19] R. Rinaldi, G. Maruccio, A. Biasco, V. Arima, R. Cingolani, T. Giorgi, S. Masiero, G. P. Spada, G. Gottarelli, *Nanotechnology* **2002**, *13*, 398; R. Rinaldi, E. Branca, R. Cingolani, R. Di Felice, A. Calzolari, E. Molinari, S. Masiero, G. Spada, G. Gottarelli, A. Garbesi, *Ann. N. Y. Acad. Sci.* **2002**, *960*, 184.
- [20] G. Maruccio, P. Visconti, V. Arima, S. D'Amico, A. Blasco, E. D'Amone, R. Cingolani, R. Rinaldi, S. Masiero, T. Giorgi, G. Gottarelli, *Nano Lett.* **2003**, *3*, 479.
- [21] K. Araki, I. Yoshikawa, *Top. Curr. Chem.* **2005**, *256*, 133.
- [22] T. D. W. Claridge, *High-Resolution NMR Techniques in Organic Chemistry*, Pergamon-Elsevier, Oxford, **1999**, Chapter 8.
- [23] T. Giorgi, S. Lena, P. Mariani, M. A. Cremonini, S. Masiero, S. Pieraccini, J. P. Rabe, P. Samori, G. P. Spada, G. Gottarelli, *J. Am. Chem. Soc.* **2003**, *125*, 14741.
- [24] In the presence of potassium ions, the CD spectrum shows a much higher signal in the guanine absorption region with an excitonlike ( $\Delta\epsilon \approx 20$ ), bisignate couplet, in accordance with previous reports on stacked G-quartet architectures: S. Pieraccini, G. Gottarelli, P. Mariani, S. Masiero, L. Saturni, G. P. Spada, *Chirality* **2001**, *13*, 7.
- [25] *International Tables of X-ray Crystallography*, The Kynoch Press, Birmingham, **1952**.
- [26] G. Gottarelli, G. P. Spada, P. Mariani, *Crystallography of Supramolecular Compounds* (Eds.: G. Tsoucaris, J. L. Atwood, J. Lipkowsky), Kluwer Academic, Dordrecht, **1996**, pp. 307–330.

- [27] A. Yazdani, C. M. Lieber, *Nature* **1999**, *401*, 227; J. K. Gimzewski, C. Joachim, *Polim. Cienc. Tecnol. Science* **1999**, *283*, 1683; P. Samorì, *J. Mater. Chem.* **2004**, *14*, 1353.
- [28] D. M. Cyr, B. Venkataraman, G. W. Flynn, A. Black, G. M. Whitesides, *J. Phys. Chem.* **1996**, *100*, 13747.
- [29] R. Otero, M. Schock, L. M. Molina, E. Laegsgaard, I. Stensgaard, B. Hammer, F. Besenbacher, *Angew. Chem.* **2005**, *117*, 2310; *Angew. Chem. Int. Ed.* **2005**, *44*, 2270.
- [30] G. C. McGonigal, R. H. Bernhardt, D. J. Thomson, *Appl. Phys. Lett.* **1990**, *57*, 28; J. P. Rabe, S. Buchholz, *Science* **1991**, *253*, 424; X. H. Qiu, C. Wang, Q. D. Zeng, B. Xu, S. X. Yin, H. N. Wang, S. D. Xu, C. L. Bai, *J. Am. Chem. Soc.* **2000**, *122*, 5550; D. M. Cyr, B. Venkataraman, G. W. Flynn, *Chem. Mater.* **1996**, *8*, 1600; S. De Feyter, F. C. De Schryver, *J. Phys. Chem. B* **2005**, *109*, 4290; P. Samorì, V. Francke, V. Enkelmann, K. Müllen, J. P. Rabe, *Chem. Mater.* **2003**, *15*, 1032.
- [31] R. Lazzaroni, A. Calderone, J. L. Brédas, J. P. Rabe, *J. Chem. Phys.* **1997**, *107*, 99.
- [32] L. Horny, N. D. K. Petraco, C. Pak, H. F. Schäfer, *J. Am. Chem. Soc.* **2002**, *124*, 5861; L. Horny, N. D. K. Petraco, H. F. Schäfer, *J. Am. Chem. Soc.* **2002**, *124*, 14716.

Received: October 16, 2006  
Published online: January 17, 2007